J. Phys. Chem., Article

Direct Evidence for Li Ion Hopping Conduction in Highly Concentrated Sulfolane-Based Liquid Electrolytes

Kaoru Dokko,[†] Daiki Watanabe,[†] Yosuke Ugata,[†] Morgan L. Thomas,[†] Seiji Tsuzuki,[‡] Wataru Shinoda,[§] Kei Hashimoto,[†] Kazuhide Ueno,[†] Yasuhiro Umebayashi,[∥] and Masayoshi Watanabe[†,*]

[†]Department of Chemistry and Biotechnology, Yokohama National University, 79-5 Tokiwadai, Hodogaya-ku, Yokohama 240-8501, Japan

[‡] Research Center for Computational Design of Advanced Functional Materials (CD-FMat), National Institute of Advanced Industrial Science and Technology (AIST), Tsukuba Central 2, 1-1-1 Umezono, Tsukuba, Ibaraki 305-8568, Japan

[§]Department of Materials Chemistry, Nagoya University, Furo-cho, Chikusa-ku, Nagoya 464-8603, Japan

[∥] Graduate School of Science and Technology, Niigata University, 8050 Ikarashi, 2-no-cho, Nishi-ku, Niigata 950-2181, Japan

*To whom correspondence should be addressed. E-mail: mwatanab@ynu.ac.jp

Abstract

We demonstrate that Li^+ hopping conduction, which cannot be explained by conventional models i.e. Onsager's theory and Stokes' law, emerges in highly concentrated liquid electrolytes composed of $LiBF_4$ and sulfolane (SL). Self-diffusion coefficients of Li^+ (D_{Li}), BF_4^- (D_{BF4}), and SL (D_{SL}) were measured with pulsed field gradient NMR. In the concentrated electrolytes with molar ratios of SL/$LiBF_4$ ≤ 3, the ratios D_{SL}/D_{Li} and D_{BF4}/D_{Li} become lower than 1, suggesting faster diffusion of Li^+ than SL and BF_4^-, and thus the evolution of Li^+ hopping conduction. X-ray crystallographic analysis of the $LiBF_4$:SL (1:1) solvate revealed that the two oxygen atoms of the sulfone group are involved in bridging coordination of two different Li^+ ions. In addition, the BF_4^- anion also participates in bridging coordination of Li^+. Raman spectra of the highly concentrated $LiBF_4$-SL solution suggested that Li^+ ions are bridged by SL and BF_4^- even in the liquid state. Moreover, detailed investigation along with molecular dynamics simulations suggests that Li^+ exchanges ligands (SL and BF_4^-) dynamically in the highly concentrated electrolytes, and Li^+ hops from one coordination site to another. The spatial proximity of coordination sites, along with possible domain structure, is assumed to enable Li^+ hopping conduction. Finally, we demonstrate that Li^+ hopping suppresses concentration polarization in Li batteries, leading to increased limiting current density and improved rate capability compared to the conventional concentration electrolyte. Identification and rationalization of Li^+ ion hopping in concentrated SL electrolytes is expected to trigger a new paradigm of understanding for such unconventional electrolyte systems.

Introduction

Ion conduction in dilute electrolyte solutions containing excess solvent is well explained by conventional solution theory.[1] In electrolyte solutions containing excess solvent, the salt dissociates into its component ions, and the ions are stabilized by solvation. The solvated ions then diffuse and migrate in the solution, via the so-called vehicular mechanism. Specifically, Onsager's theory well describes the ion conduction in dilute strong electrolyte solutions. The ionic conductivity can be related to the diffusion coefficients of the ions by the Nernst-Einstein equation. The diffusion coefficients of ions are described by the Stokes-Einstein equation (valid for diffusion of species in a homogeneous medium). Therein, the diffusion coefficients of the ions are proportional to $1/\eta$ (η: viscosity) and $1/r_h$ (r_h: hydrodynamic radius of the ionic species). In the case of electrolytes composed of Li salt and aprotic solvents, the Li^+ ion is solvated by aprotic solvent molecules, and the solvated Li^+, i.e., $[Li(solvent)_x]^+$, is formed in solution.[2] The solvated Li^+ ion then diffuses in the solution, and therefore, the effective hydrodynamic radius of Li^+ becomes much larger than the typical crystallographic ionic radius of Li^+.[3]

Organic electrolytes containing Li salts are employed practically in Li-ion batteries (LIBs), and their physicochemical properties have been widely studied.[4-5] Commonly used electrolytes for LIBs contain ca. 1 mol dm^{-3} Li salt (typically, $LiPF_6$), because the ionic conductivity becomes highest at ~1 mol dm^{-3} (*vide infra*). However, highly concentrated electrolytes containing Li salt with concentrations of greater than 3 mol dm^{-3}, termed "solvent-in-salt" or "superconcentrated" electrolytes, have recently attracted much attention owing to their unique physicochemical properties and their potential applications to next generation batteries.[6-11] The highly concentrated electrolytes are known to possess wide electrochemical windows and expected to be used in high voltage batteries.[12-14] Here, we note that compared with other aprotic solvents, sulfones are known to have higher oxidative stability and have been

investigated as electrolyte solvents for LIBs.[15-22] In addition, highly reversible Li metal deposition/dissolution in the highly concentrated sulfone-based electrolytes were reported recently.[23] Such electrolytes are expected to be suitable for development of high-voltage and high-energy-density batteries.[22-23]

In this study, we investigated the transport properties of highly concentrated electrolytes composed of Li salts and sulfolane (SL). In the highly concentrated electrolytes, almost all solvent molecules in solution are involved in the solvation of Li^+ ion, and thus the proportion of uncoordinated (free) solvent molecules is negligible. Moreover, the solvated Li^+ ions are always in close proximity to the anions, leading to strong electrostatic interactions between Li^+ and anions. This situation is completely different from that of dilute electrolyte solution, and thus Onsager's theory and Stokes law cannot reasonably be applied to the highly concentrated electrolytes. We found that Li^+ hopping conduction, akin to the Grotthuss mechanism in protic media, occurs in the highly concentrated SL-based electrolytes. An ion conduction mechanism in the solvent-in-salt electrolytes is proposed based on the solvation structure of Li^+ and molecular dynamics (MD) simulations. Finally, we demonstrate that the Li^+ hopping suppresses the concentration polarization in Li batteries.

Results and Discussion

Transport properties. The ionic conductivity (σ) and viscosity (η) of $LiBF_4$-SL electrolyte as a function of concentration are shown in **Figure 1a** and **Table S1** (Supporting Information). The ionic conductivity of $LiBF_4$-SL electrolyte increases with increasing concentration of $LiBF_4$ up to ~ 1 mol dm^{-3}, because the charge carrier density increases as concentration increases. A further increase in concentration leads to a decrease in ionic conductivity due to the increase in viscosity of the electrolyte solutions, which impedes the mobility of each component species. **Figure 1b** shows the self-diffusion coefficients of Li^+

(D_{Li}), BF_4^- (D_{BF4}), and SL (D_{SL}) measured using pulsed field gradient (PFG) NMR. At around a concentration of 1 mol dm^{-3}, the relative order of self-diffusion coefficients is as follows: $D_{SL} > D_{BF4} > D_{Li}$, as is the case for conventional organic electrolytes for LIBs.[24-25] This is because the Li^+ is solvated by SL in the electrolyte and forms $[Li(SL)_x]^+$ complexes. According to the Stokes-Einstein equation, the diffusion coefficient of each species is proportional to $1/\eta$ and $1/r_h$. The r_h of the solvated Li^+, $[Li(SL)_x]^+$, is larger than those of the free SL and the BF_4^- anion. It should be noted that NMR could not distinguish the free SL and the bound SL in the $[Li(SL)_x]^+$ complex, suggesting that the Li^+ exchanges ligands, i.e., SL, rapidly in the electrolyte. This is because the lifetime of monodentate-type solvents in the first solvation shell of Li^+ is in the order of 10^{-9} s,[2, 26] while the time scale for NMR measurements is ~10^{-4}–10^{-2} s. Therefore, the measured D_{SL} is the average value of free and coordinated SL molecules. At concentrations higher than 3 mol dm^{-3}, the viscosity increases dramatically with the $LiBF_4$ concentration, and the self-diffusion coefficient of each species was one order of magnitude lower than that in 1 mol dm^{-3} solution. Although the mobility of each species was low, a surprising phenomenon was observed. **Figure 1c** shows the ratios of self-diffusion coefficients D_{SL}/D_{Li} and D_{BF4}/D_{Li} as a function of concentration. Both the D_{SL}/D_{Li} and D_{BF4}/D_{Li} decrease upon increasing the $LiBF_4$ concentration (decreasing the molar ratio of SL/$LiBF_4$). The decrease in D_{BF4}/D_{Li} indicates that the transference number of Li^+ (t_{Li+}) increases with $LiBF_4$ concentration in the electrolyte solution. In the concentrated electrolytes with molar ratios of SL/$LiBF_4 \leq 3$, the D_{SL}/D_{Li} and D_{BF4}/D_{Li} are below unity, suggesting that Li^+ diffuses faster than the SL molecule and BF_4^- anion. Similar results were obtained for the SL-based highly concentrated electrolytes containing other Li salts, such as $LiClO_4$ and $LiN(SO_2F)_2$ (Li[FSA]) (**Figures S1 and S2**, and **Tables S2 and S3**, Supporting Information). Namely, D_{Li} is higher than D_{SL} in these electrolyte solutions when the molar ratio of SL/Li salt is lower than 3. Although unfortunately, the diffusivity of ClO_4^- in the $LiClO_4$-SL electrolyte could not be

measured using the PFG-NMR apparatus employed in this study, we could also confirm that Li^+ diffuses faster than the $[FSA]^-$ anion in the highly concentrated Li[FSA]-SL electrolyte. Very recently, Alvarado et al. also reported that Li^+ diffuses faster than SL and the anion in highly concentrated Li[FSA]-SL solutions,[22] and this agrees well with our observation (**Figure S2**). These results suggest that the Stokes-Einstein equation is no longer valid for the $[Li(SL)_x]^+$ complex cation in the highly concentrated Li salt-SL solutions. In general, the coordination number of Li^+ in electrolyte solutions is 4-5.[27] The fraction of free solvent (SL) in the solution is lowered with increasing Li salt concentration. In this situation, not only SL but also BF_4^- are assumed to be coordinated to Li^+, in other words, aggregates (AGGs) such as $[Li_x(SL)_y(BF_4)_z]^{x-z}$ (where x= 1 or more) might be formed in the electrolytes. We undertook detailed analyses (*vide infra*) of the solvation structure in order to understand the appearance of Li^+ ion hopping in these concentrated solutions.

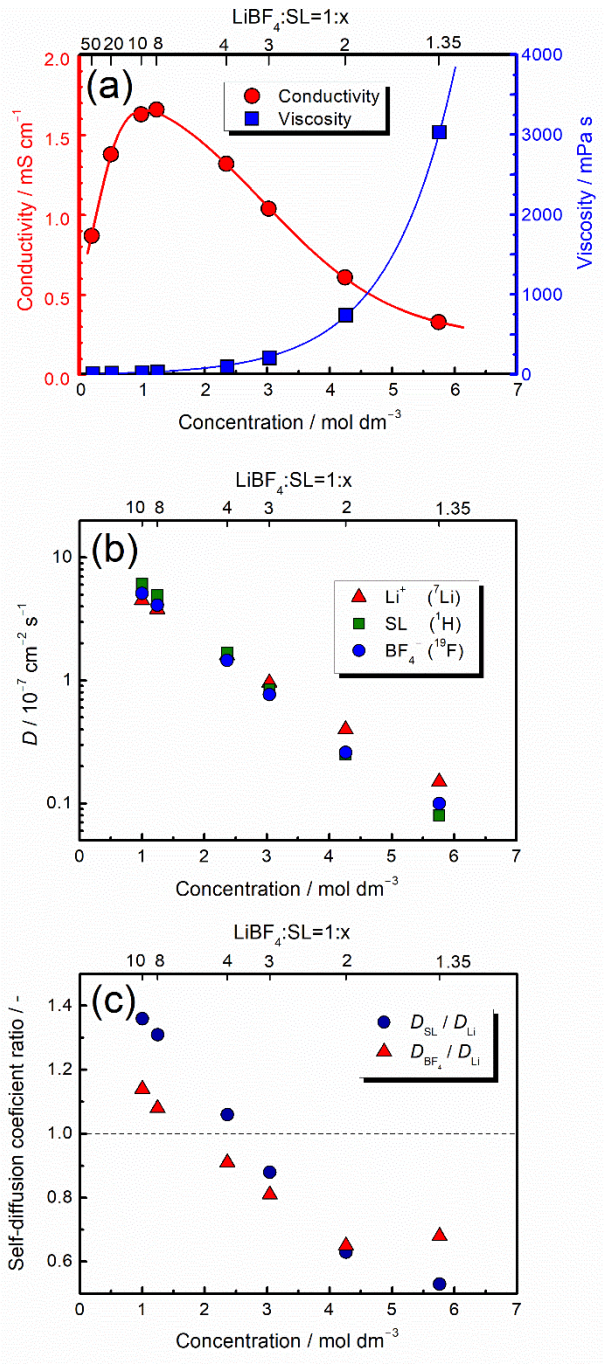

Figure 1. (a) Ionic conductivity and viscosity (lines are a guide for the eye), (b) self-diffusion coefficients of Li^+ (D_{Li}), BF_4^- (D_{BF4}), and SL (D_{SL}), and (c) ratios of self-diffusion coefficients D_{SL}/D_{Li} and D_{BF4}/D_{Li} of $LiBF_4$-SL electrolytes at 30 °C.

Solvation structure. Differential scanning calorimetry (DSC) thermograms, and the resulting plot of glass transition temperatures (T_g) and melting points (T_m) of binary mixtures of $LiBF_4$ and SL are shown in **Figure S3**. The melting point (T_m) of pure SL is 27.5 °C, and the T_m of the mixture decreases as the mole fraction of $LiBF_4$ increases. The highly

concentrated mixtures of $LiBF_4$:SL= 1:2 and 1:3 are glass forming liquids and melting points were not observed. These two mixtures maintain a liquid state at room temperature. The mixture of $LiBF_4$:SL=1:1 can be crystallized, and has a T_m of 39.7 °C. The crystal structure of the $LiBF_4$:SL=1:1 solvate was analyzed using single crystal X-ray diffraction (**Figure S4 and Table S4**). In the crystal, the coordination number of Li^+ is 4, as shown in **Figure 2a**. The two oxygen atoms of a single SL molecule are involved in the bridging coordination of two different Li^+ ions. In addition, the BF_4^- anion also participates in the bridging coordination of two Li^+ ions. For comparison, the crystal structures of solvates of Li[FSA]-SL and $LiClO_4$-SL were also determined. Li[FSA] also forms a stable solvate with SL in a 1:1 molar ratio (T_m = 75 °C) (**Figure S5**), and in the crystal the SL molecule bridges Li^+ ions (**Figure S6 and Table S5**), similar to the case of the $LiBF_4$:SL=1:1 crystal. In contrast, rather than the 1:1 solvate observed for $LiBF_4$, $LiClO_4$ forms a solvate with SL in a 1:2 molar ratio (T_m = 55 °C) (**Figure S7**), despite the fact that both the BF_4^- and ClO_4^- anions have a tetragonal geometry and similar anion size.[28-29] Interestingly, in the $LiClO_4$:SL=1:2 crystal (**Figure S8 and Table S6**), 50% of SL molecules act as simple monodentate ligands for Li^+, and the remaining 50% of SL molecules bridge different Li^+ ions. The ClO_4^- anion also participates as a monodentate ligand in the coordination of Li^+ (**Figure 2b**).

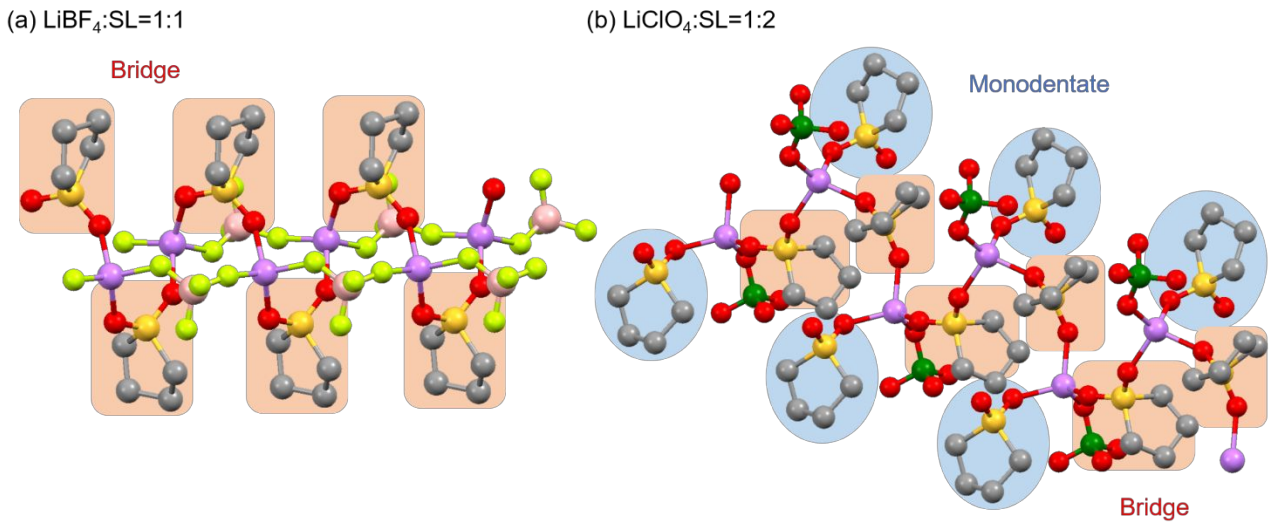

Figure 2. Ball and stick models for $LiBF_4$:SL=1:1 (a) and $LiClO_4$:SL=1:2 (b) crystals. Hydrogen atoms are not shown. Purple, Li; red, O; gray, C; yellow, S; light green, F; pink, B; green, Cl. The crystallographic information file (cif) for (a) was deposited in the Cambridge Structure Database (CSD) as CCDC 1866668.

Figure 3 shows the Raman spectra in the spectral range corresponding to the SO_2 scissoring vibration of SL.[30] This peak appears at 568 cm^{-1} in neat SL, and shifts to higher wavenumber upon complexation with Li^+. As shown in **Figure 3**, the crystals of $LiBF_4$:SL=1:1 showed a relatively sharp peak at 576 cm^{-1} while $LiClO_4$:SL=1:2 exhibited two peaks at 571 and 580 cm^{-1}. Taking into account both the crystal structures and Raman spectra, the SO_2 vibration observed at 576 cm^{-1} for the solid state $LiBF_4$:SL=1:1 is assigned to the sulfone group coordinating to different Li^+ ions (i.e. bridging type SL). The two peaks at 571 and 580 cm^{-1} for the $LiClO_4$:SL=1:2 crystal correspond to the two types of SL, i.e., monodentate and bridging types, in the crystal. Specifically, the higher wavenumber peak (580 cm^{-1}) was attributed to the bridging type SL, and the lower wavenumber peak (571 cm^{-1}) was attributed to the SL coordinated to only one Li^+ ion as a monodentate ligand (**Figure 2**). As shown in **Figure 3**, the peaks corresponding to the SO_2 scissoring vibration for $LiBF_4$:SL=1:1 and $LiClO_4$:SL=1:2 were broadened upon melting, indicating that the solvation structures change dynamically in the liquids. In the spectrum for $LiClO_4$:SL=1:2 in the liquid state, the two peaks

at 571 and 580 cm^{-1} overlapped significantly, and the peak area of 571 cm^{-1} became larger than that of 580 cm^{-1} (**Figure S9**), suggesting that the proportion of monodentate SL increased with melting (**Table S7**). In addition, the tailing of the peak to lower wavenumber ~560 cm^{-1} indicates that free SL, which is not bound to Li^+, was generated upon melting. In the case of $LiBF_4$:SL=1:1, the SO_2 peak shifted slightly to lower wavenumber upon melting (**Figure 3**). This implies that some portion of the bridging type SL changed to the monodentate type; however, a significant amount of bridging type SL was still present. The Raman spectrum of $LiBF_4$:SL=1:2 solution also exhibits a broadened peak in the range 565~590 cm^{-1}. It is thus clear that a certain proportion of SL behaves as a bridging ligand in addition to monodentate coordination, in the liquid (**Figure S10, Table S8**). We note here that the fitting results shown in Figures S9, S10 and Tables S7, S8 can only provide an approximation of the relative proportions of the various coordination types.

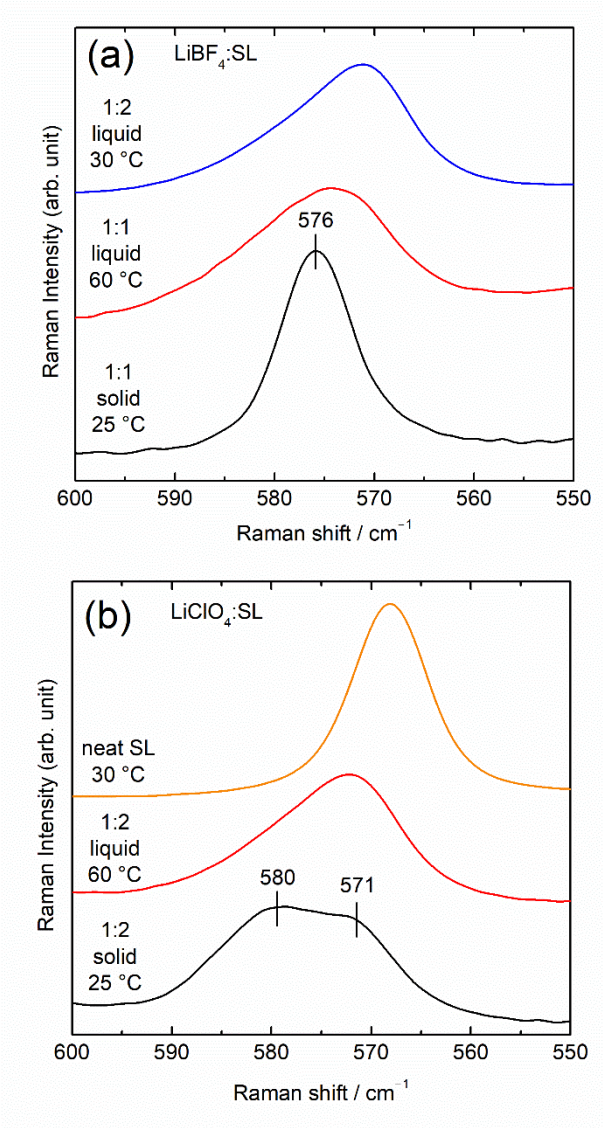

Figure 3. Raman spectra in the region of the scissoring mode of SO_2 group of SL in $LiBF_4$-SL (a) and $LiClO_4$-SL (b).

Similarly, the characteristic Raman bands for the anions provide information regarding the interaction between Li^+ and the anions in the Li salt-SL electrolytes. The Raman spectrum of the $LiBF_4$:SL=1:1 solvate (crystal) is shown in **Figure 4a**. The band observed at 775 cm^{-1}, which is the B−F symmetric stretching mode, is assigned to the specific coordination and geometry of BF_4^- in the aggregated structure, where two fluorine atoms of a BF_4^- anion are involved in the coordination of different Li^+ ions, i.e. BF_4^- anion bridges Li^+ ions (**Figure 2a**). Upon melting, the BF_4^- peak becomes broader, suggesting that the aggregated structure of Li-

BF_4 changed. We also note here the melting of the crystal itself would be expected to contribute to the observed broadening, the shift of the peak maximum also suggests changes in the coordination structures. According to Henderson et al., the Raman band of BF_4^- anion changes depending on the number of Li^+ ions bound to a single BF_4^- anion.[31] Specifically, free or solvent separated ion pair (SSIP) type BF_4^- anion exhibits a peak in the range 764−765 cm^{-1}, and BF_4^- forming a contact ion pair (CIP) bound to only one Li^+ shows a peak at 767 cm^{-1}. In addition, BF_4^- bound to two Li^+ ions (AGG-I type BF_4^-) shows a band at ~ 777−779 cm^{-1}, and the band of BF_4^- bound to three Li^+ ions (AGG-II type BF_4^-) locates over a wide range of ~776−788 cm^{-1}. Therefore, the broadening of the anionic peak by melting suggests that some portion of the AGG-I type BF_4^- observed in the crystal was transformed into AGG-II type. This is because the population of bridging type SL decreases with melting of $LiBF_4$:SL=1:1 (vide supra), and thus BF_4^- anions should be involved in the coordination of more than two Li^+ ions to satisfy the preferred coordination number of Li^+. Similar to the case of $LiBF_4$:SL=1:1, the solvation structure of $LiClO_4$:SL=1:2 changed upon melting. As shown in **Figure S11**, the Raman peak of ClO_4^- observed for the $LiClO_4$:SL=1:2 crystal at 934 cm^{-1}, which is assigned to the Cl−O symmetric stretching mode of ClO_4^-, shifted to higher wavenumber upon melting. In the crystal of $LiClO_4$:SL=1:2, ClO_4^- is bound to only one Li^+ i.e. monodentate. The shift of ClO_4^- peak to higher wavenumber suggests that a ClO_4^- binds to more than one Li^+ ion in the liquid.[32] Again, this is because the population of bridging type SL decreases upon melting of $LiClO_4$:SL=1:2 (vide supra).

Figure 4b shows the Raman spectra in the range of 720−820 cm^{-1} for $LiBF_4$-SL mixed at various molar ratios. The Raman band for the symmetric vibration of BF_4^- is observed at 766 cm^{-1} for $LiBF_4$:SL=1:10 (i.e. 1.0 mol dm^{-3} $LiBF_4$-SL, see **Table S1**). For the concentrated solutions, $LiBF_4$:SL=1:3 and 1:2, the peak showed a shoulder and the peak at 775 cm^{-1} become prominent, although the band corresponding to the CH_2 rocking mode of SL at 788 cm^{-1}

overlaps. As previously mentioned, the Raman band of BF_4^- is sensitive to the formation of aggregated structures of Li^+ and BF_4^-. The intense peak observed at 775 cm^{-1} indicates the formation of AGGs in the liquid electrolytes. Consequently, it was revealed that a significant proportion of AGGs, where BF_4^- is bound to two or more Li^+ ions, are formed in the liquids with bulk compositions of $SL/LiBF_4 \leq 3$.

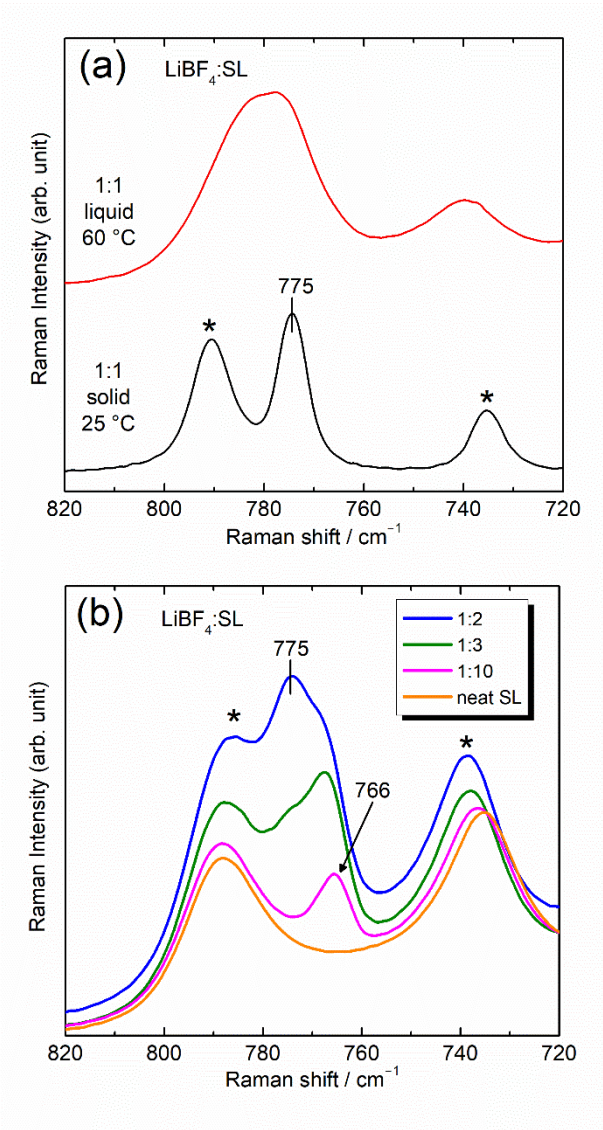

Figure 4. Raman spectra of BF_4^- in the $LiBF_4$:SL = 1:1 (a), and $LiBF_4$-SL binary mixtures with various molar ratios ($LiBF_4$:SL = 1:*x*) (b). The peaks (*) at 735 and 790 cm^{-1} are the C-S-C antisymmetric stretching and CH_2 rocking vibration modes of SL, respectively.[30]

Li^+ hopping conduction mechanism. The fact that D_{Li} is larger than D_{SL} and D_{BF4} in the $SL/LiBF_4 \leq 3$ electrolytes (**Figure 1**) strongly suggests that Li^+ exchanges between the

coordination sites formed by the ligands (SL and BF_4^-) and moves forward leaving behind the ligands. In other words, Li^+ hopping conduction occurs in the liquids. Note that the hopping conduction is observed in the highly concentrated SL-based electrolytes containing other Li salts, such as $LiClO_4$ and Li[FSA] (**Figures S1 and S2**). The proton hopping conduction mechanism (Grotthuss mechanism) in acidic and basic aqueous solution is well known; however, the hopping conduction of metal ions in liquids has not been well recognized so far. To date, it is known that hopping conduction of Li^+ occurs in solid electrolytes such as inorganic solid electrolytes and polymer electrolytes. In the Li^+ ion conducting inorganic solid electrolytes, the positions of ligands, such as oxide ions and sulfide ions, are fixed; however, the coordination sites are closely placed, and Li^+ ion can hop from one coordination site to the nearest vacant site.[33-34] In polymer electrolytes, the segmental motion of the polymer chain induces the ligand exchange of Li^+, and the Li^+ hopping conduction takes place.[33] Another mechanism, concentration-dependent percolation-type diffusion of ions, was also proposed for polymer-in-salt type electrolytes.[35-36] Regarding the transport properties of aprotic liquid electrolytes, several groups proposed a Grotthuss-type (hopping-type) conduction mechanism of alkali metal ions in electrolytes containing high concentrations of alkali metal salts.[12, 37-41] They reported that the transference number of alkali metal ion (A^+) was increased with increasing salt concentration in the liquid electrolytes. In the highly concentrated electrolytes, the formation of aggregated structures, such as $[A_x(\text{solvent})_y(\text{anion})_z]^{x-z}$ (where x= 1 or more) occurred, and the increase in the transference number of A^+ was speculated to be due to the ligand exchange of A^+ in the aggregated structures. MD simulation studies supported the postulation that ligand exchange of the alkali metal ion in the highly concentrated electrolytes contributes to the transport.[22, 38-40]

Our present experimental data, the higher diffusion coefficient of Li^+ than that of SL and anions (**Figure 1, Figures S2 and S3**), provides direct evidence that Li^+ hopping

conduction occurs in the highly concentrated SL-based electrolytes with molar ratios of SL/Li salt ≤ 3. In the case of highly concentrated Li salt-SL solution, the viscosity is rather high, and this compels the SL and anions to transport considerably slowly. In addition, both of the two oxygen atoms of the SL (SO_2 group) can contribute to the coordination of Li^+ ions as revealed by X-ray crystallography (**Figure 2**) and Raman spectroscopy (**Figure 3**). These provide closely placed coordination sites for Li^+ ions. Furthermore, the high concentration of anion in the electrolyte can also provide a vast number of coordination sites. These factors are considered to cooperatively promote the Li^+ hopping conduction and increase the t_{Li+} in highly concentrated SL-based electrolytes. Here we also note that MD simulations supported our experimental findings i.e. that the ligand exchange and Li^+ hopping conduction occur in the highly concentrated electrolytes (**Figures S12-S17** and **Tables S9-S12**, Supporting Information). MD simulation reproduced the higher diffusion coefficient of Li^+ than those of SL and BF_4^- in the highly concentrated $LiBF_4$-SL electrolytes. Li^+ ions are dispersed in SL when the concentration of $LiBF_4$ salt is low ($LiBF_4$:SL = 1:8) as shown in **Figure S17(a)** (Supporting Information). On the other hand, Li^+ ions, BF_4^- anions and SO_2 groups of SL molecules form aggregates (polar domain) and the methylene groups of SL molecules form aggregates (nonpolar domain) in the mixture when the concentration of $LiBF_4$ salt is high ($LiBF_4$:SL = 1:2) as shown in **Figure S17(b)** (Supporting Information), which suggests that nano-phase separation occurs in the mixture at high $LiBF_4$ concentrations. The concentration dependence of the liquid structure of the mixture suggests that the formation of the polar domain plays an important role in the evolution of Li^+ hopping conduction.

Electrochemical properties. To further investigate the Li^+ ion transport in the SL-based electrolytes, electrochemical measurements were carried out. Cyclic voltammetry was initially performed, demonstrating that the lithium deposition/dissolution processes are both observed in a concentrated $LiBF_4$-SL electrolyte (**Figure S18**). We note here that efficient

cycling of a lithium metal anode in a concentrated Li[FSA]-SL mixture was recently reported.[23] Chronoamperometry (CA) was performed in symmetric cells i.e. [Li metal | electrolyte | Li metal], where-in the negative and positive electrodes were separated with 4 sheets of porous polyolefin film (Celgard 3501), and the distance between the electrodes was 100 μm. **Figure 5a** shows the current responses of the cell with $LiBF_4$:SL=1:10 electrolyte measured at various applied voltages. Upon increasing the voltage, the current increases owing to the increase in the charge transfer rate at the Li metal electrodes. The current decayed with time up to 200 s after voltage application, and a steady state current was observed after 200 s. During the CA measurements, electrodeposition and dissolution of Li metal occur at the negative and positive electrodes, respectively, while the anion, BF_4^-, cannot be discharged at the electrodes. The t_{Li+} is less than 1 in liquid electrolytes, and this causes the concentration polarization of $LiBF_4$ in the cell.[42] Through electrochemical reactions at the negative and positive electrodes, a concentration gradient of $LiBF_4$ is formed in the vicinity of the electrodes. The growth of the diffusion layer from the negative electrode to positive electrode, across the electrolyte, completed within 200 s and reached the steady state. The steady state current increased with increasing the applied voltage up to 400 mV, however, became constant (2.5 mA cm^{-2}) and independent of the voltage at higher than 450 mV, suggesting that the Faradaic current reached the Li^+-diffusion limiting current density. Under the diffusion limiting condition, it is assumed that the depletion of $LiBF_4$ occurs at the negative Li metal electrode, and the limiting current density can be roughly calculated, based on the diffusion coefficient of Li^+, to be 1.5 mA cm^{-2} (**Table S13**, Supporting Information), which similar in magnitude to the experimentally observed value (2.5 mA cm^{-2}). In this way, concentration polarization occurs at high current density in the electrolyte containing excess SL ($LiBF_4$:SL =1:10), and the maximum electrochemical reaction rate is limited by the chemical diffusion of Li^+.

To investigate the effect of Li^+ hopping conduction on the electrochemical reaction rate,

analogous CA measurements were carried out for a Li/Li symmetric cell with $LiBF_4$:SL=1:2 (**Figure 5b**). At each voltage, the Faradaic current is observed from the moment the voltage is applied to the cell, and the current is more or less constant and time independent. This behavior is in stark contrast to that of the cell with $LiBF_4$:SL =1:10 (**Figure 5a**). The time independent current suggests that the growth of the concentration polarization in the $LiBF_4$:SL=1:2 electrolyte was not so remarkable after the start of electrolysis, regardless of the production and consumption of Li^+ at the positive and negative electrodes, respectively. In other words, the chemical diffusion of Li^+ (i.e. due to concentration gradient) in the electrolyte makes less contribution to the current, and the concentration polarization was greatly suppressed. This is likely because the Li^+ ion migration through hopping conduction makes a larger contribution to the current than that of the chemical diffusion. We note here that a slight increase of current with time was observed for the concentrated electrolyte (**Figure 5b**). This slight increase of the current might be due to the decrease of the interfacial resistance at the initial stage of the electrolysis. The electrodeposition and dissolution of Li metal would cause the roughening of the electrodes. The roughening of the electrode surface increases the surface area of the electrodes, leading to the decrease of charge transfer resistance for the electrochemical reaction and the increase of the migration current in the electrolyte solution. When Li^+ hopping transport occurs in the electrolyte, the t_{Li+} becomes larger, and the contribution of the anion to the charge transport becomes smaller. Strikingly, the D_{BF4}/D_{Li} decreases with increasing $LiBF_4$ concentration in the electrolytes (**Figure 1c**), indicating that the t_{Li+} increases with $LiBF_4$ concentration. In addition, the t_{Li+} estimated by an electrochemical method also showed the same concentration-dependent trend (**Figure S19**, **Table S14**). The higher t_{Li+} results in a gentle slope of Li salt concentration gradient in the electrolyte during the electrolysis.[42-43] The extreme case of this situation is a typical inorganic Li^+ ion conductor, in which the position of anion is fixed and t_{Li+} =1, and the concentration gradient of Li^+ ion is hardly formed. In the

case of migration-controlled Li^+ transport, the current should increase with increasing applied voltage. Indeed, the steady state current for the symmetric cell with $LiBF_4$:SL=1:2 electrolyte continuously increased with increasing applied voltage, and the steady-state current observed for the cell at 700 mV was as high as 3.5 mA cm^{-2}. Note that the ionic conductivity of $LiBF_4$:SL = 1:2 is 0.61 mS cm^{-1}, notably lower than that of $LiBF_4$:SL = 1:10 (1.63 mS cm^{-1}); nevertheless a higher current density can be achieved in $LiBF_4$:SL =1:2 (**Figure 5c**). We note here that the dendritic growth of Li metal occurs at the negative electrode with a polarization higher than 700 mV. This resulted in the internal short circuit of the cell, and unfortunately reproducible data could not be obtained at higher than 700 mV.

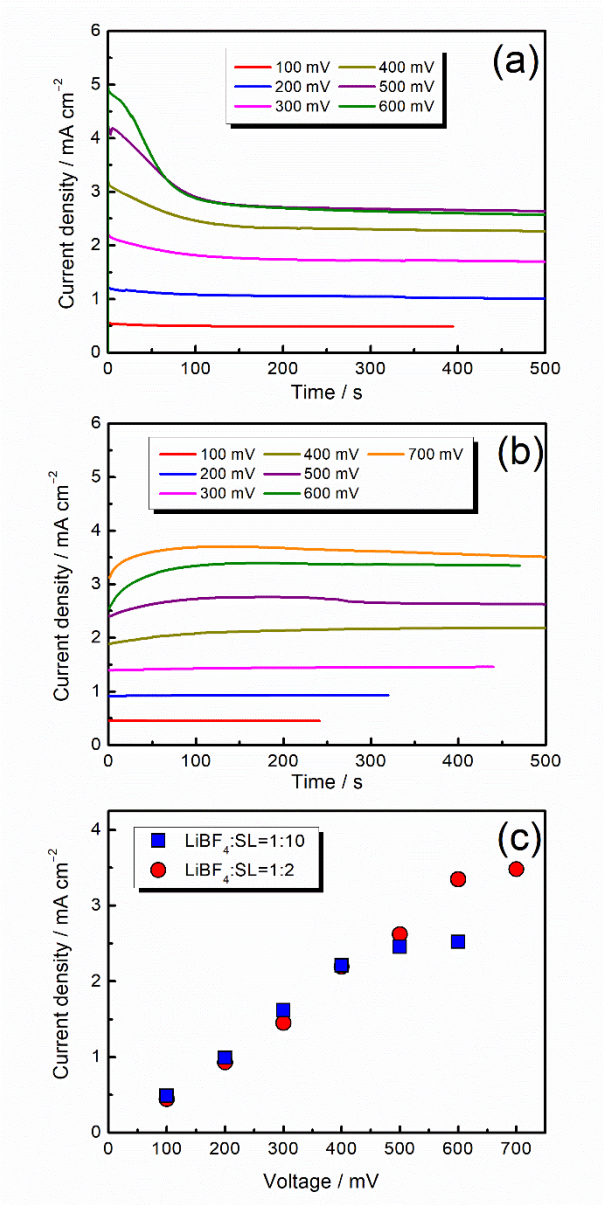

Figure 5. Chronoamperograms for symmetric [Li | $LiBF_4$-SL with 4 sheets of Celgard 3501 (100 μm) | Li] cells measured at various applied voltages at 30 °C. The electrolyte compositions were with $LiBF_4$:SL= 1:10 (a) and 1:2 (b). Dependences of steady state current densities of the symmetric cells on the applied voltage (c).

Finally, we examined the effects of the Li^+ ion transport properties of the electrolytes on Li battery performance. **Figure 6** shows the discharge rate capabilities of Li/$LiCoO_2$ cells with $LiBF_4$:SL = 1:2 and 1:10 electrolytes. The discharge curves measured at various current densities are shown in **Figure S20**. At low current densities, both cells showed a discharge capacity of ca. 140 mAh g^{-1}, which is close to the theoretical capacity of $LiCoO_2$. With

increasing current density, the discharge capacities of the cells decreased owing to the Li^+ transport limitation in the electrolytes. The discharge capacity of the cell with $LiBF_4$:SL = 1:10 was as low as 20 mAh g^{-1} at 2.65 mA cm^{-2}. This is because the current density is close to the limiting current of $LiBF_4$:SL = 1:10. On the other hand, the cell with $LiBF_4$:SL=1:2 showed a capacity of 80 mAh g^{-1} at 2.65 mA cm^{-2}. The superior rate capability of the cell with $LiBF_4$:SL=1:2 electrolyte is ascribed to the higher limiting current and the suppressed concentration polarization. The ionic conductivity of the $LiBF_4$:SL=1:2 is not so high at room temperature owing to its high viscosity. However, with increasing the temperature, the viscosity of the liquid decreases and the ionic conductivity increases (**Figure S21** and **Table S15**, Supporting Information). Even at the elevated temperature (~ 90 °C), Li^+ diffuses faster than BF_4^- and SL, i.e., the hopping conduction of Li^+ occurs (**Figure S22**). In addition, with increasing the temperature, the higher limiting current density in an electrochemical cell can be achieved (**Figure S23**). This may be instrumental to further improve the power density of lithium batteries.

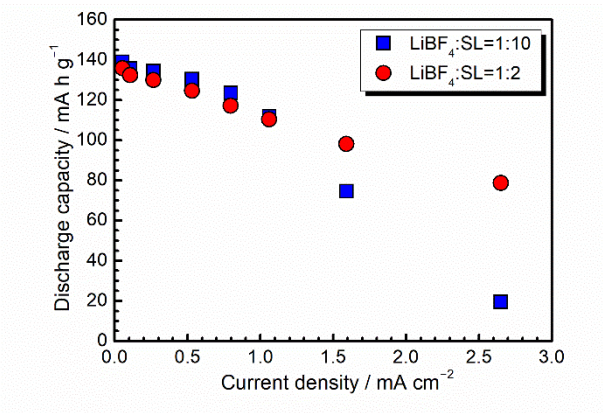

Figure 6. Discharge capacities of [Li | $LiBF_4$-SL with 2 sheets of Celgard 3501 (50 μm) | $LiCoO_2$] cells measured at various current densities at 30 °C. The cells were fully charged prior to each discharge measurement at a low current density of 53 μA cm^{-2}.

Conclusions

In this study, we elucidated the liquid structures and transport properties of highly

concentrated $LiBF_4$-SL electrolytes. In the electrolytes with compositions of SL/$LiBF_4 \leq 3$, Li^+ diffuses faster than both the SL solvent and BF_4^- anion. We demonstrated that the Li^+ hopping conduction through ligand exchange occurs in the highly concentrated electrolytes. Both SL and BF_4^- anion function as ligands for Li^+ ions. The oxygen atoms of the sulfone moiety (SO_2) of a SL molecule coordinate to different Li^+ ions and bridge them. In addition, the BF_4^- anions also bridge different Li^+ ions. The SL and BF_4^- provide closely placed coordination sites in the highly concentrated electrolytes. Li^+ ion hops from one coordination site to another with ligand exchange in the liquid. In addition, we found that Li^+ hopping conduction occurs in the highly concentrated SL-based electrolytes containing other Li salts, such as $LiClO_4$ and Li[FSA]. The Li^+ hopping conduction was effective in suppressing the concentration polarization in a lithium battery. Identification and rationalization of Li^+ ion hopping in the concentrated SL electrolytes is expected to trigger a new paradigm of understanding for such unconventional electrolyte systems.

EXPERIMENTAL SECTION

Purified SL, $LiBF_4$, $LiClO_4$, and Li[FSA] were purchased from Kishida Chemical and used as received. SL and Li salts were mixed in a glove box filled with argon gas (VAC, [H_2O] < 1 ppm). The mixtures were stirred for 24 h at room temperature, and homogeneous liquids were obtained. The detailed compositions of the electrolytes are shown in **Tables S1-S3** (Supporting Information). The liquids were stored and handled in the glove box. The ionic conductivities (σ) of electrolytes were determined by the complex impedance method using an impedance analyzer (VMP3, Biologic) in the frequency range of 500 kHz–1 Hz with a sinusoidal alternating voltage amplitude of 10 mV root-mean-square (rms). A cell equipped with two platinized platinum electrodes (CG-511B, TOA Electronics) was utilized for the conductivity measurements, and the cell constant was determined using a 0.01 M KCl aqueous

solution at 25 °C prior to the measurements. The cell was placed in a temperature-controlled chamber and conductivity was measured at 30 °C. The liquid density and viscosity were determined using a viscometer (SVM 3000, Anton Paar).

PFG-NMR measurements were carried out to determine the self-diffusion coefficients of the SL, Li^+, and BF_4^- in the electrolytes. A JEOL-ECX 400 NMR spectrometer with a 9.4 T narrow-bore super-conducting magnet equipped with a pulsed-field gradient probe and current amplifier was used for these measurements. Self-diffusion coefficients were calculated with the Hahn spin-echo sequence using the ^{1}H signals of SL, ^{7}Li signal of Li^+, and the ^{19}F signal of BF_4^-. The detailed experimental procedures have been reported elsewhere.[44] The diffusion echo signal attenuation, E, is related to the experimental parameters by the Stejskal equation[45] with a sinusoidal pulsed-field gradient:

$$\ln(E) = \ln\left(S \big/ S_{\delta=0}\right) = \frac{-\gamma^2 g^2 D \delta^2 (4\Delta - \delta)}{\pi^2}$$

where S is the spin-echo signal intensity, δ is the duration of the field gradient with magnitude g, γ is the gyromagnetic ratio, and Δ is the interval between the two gradient pulses. The values of Δ and δ were set to 50 ms and 5 ms, respectively, whereas g was set to 0.01~1.9 T m^{-1} depending on the electrolyte. The sample was inserted into an NMR microtube to a height of 3 mm to exclude convection. All measurements were conducted at 30 °C. Each sample was placed in a sample tube with an outer diameter of 4 mm, and that tube was inserted into a 5 mm standard NMR sample tube.

The thermal properties of the binary mixtures of Li salts and SL were evaluated by differential scanning calorimetry (DSC) using a DSC6220 (Seiko). The samples for DSC were sealed in aluminum pans in the glovebox. The sample pans were first heated to appropriately high temperatures to avoid thermal hysteresis, followed by cooling to −150 °C and finally heating to 100 °C at a rate of 5 °C min^{-1}. The thermograms in the final heating process were analyzed. The T_m and glass transition temperature (T_g) were estimated from the maxima of the

endothermic peaks and the onsets of the changes in heat capacities, respectively.

Single crystal X-ray structure analysis was performed on a Rigaku Mercury70 or XtaLab P2000 diffractometer using monochromatic Mo Kα radiation (λ = 0.71073 Å). Single crystals of the solvates $LiBF_4$:SL=1:1, $LiClO_4$:SL=1:2, and Li[FSA]:SL=1:1 were successfully grown in the liquids of binary mixtures of $LiBF_4$:SL=1:1, $LiClO_4$:SL=1:2.5, and Li[FSA]:SL =1:1.5, respectively. The single crystals were coated with vacuum grease to prevent contact with air, and mounted on a glass pin. The diffraction was measured at low temperature using a steady flow of −50 °C nitrogen gas. An empirical absorption correction was applied to the obtained data using multiscan averaging of symmetry equivalent data using spherical harmonics, implemented in the SCALES3 ABSPACK scaling algorithm (CrysAlisPro 1.171.38.43, Rigaku Oxford Diffraction, 2015). The crystallographic structure was solved by the direct method with SHELXT and all non-hydrogen atoms were refined anisotropically by the full-matrix least-squares method using SHELXL-2014/7.[46-47] All hydrogen atoms were placed at geometrically ideal positions and refined using an appropriate riding model. The crystallographic data are summarized in **Tables S4-S6**. Raman spectra of the electrolytes were collected using a Raman spectrometer equipped with a 532 nm laser (RMP-330, JASCO). The instrument was calibrated using a polypropylene standard. The spectral resolution was 4.5 cm^{-1}. The sample temperature was controlled using a Peltier microscope stage (TS62, Instec) with a temperature controller (mK1000, Instec).

For the cyclic voltammetry tests, a [Li foil | electrolyte | Cu foil] coin cell was constructed in the glove box, and the voltage was swept from open-circuit voltage to -0.5 V vs. Li/Li^+ and then reversed to 2.5 V vs. Li/Li^+, with a scan rate of 5 mV s^{-1} at 30 °C. For the estimation of limiting current density, symmetrical [Li metal | electrolyte | Li metal] cells were fabricated in the glove box. Li metal foil was purchased from Honjo Metal and cut into a disk shape (16 mm in diameter). 4 sheets of porous polyolefin film (Celgard 3501, 25 μm thick,

porosity: 55%) were inserted between the two Li metal electrodes (a relatively large number of separator sheets was required to alleviate lithium dendrite formation during the measurements). The Li metal electrodes and an electrolyte were encapsulated into a 2032-type coin cell in the glove box. The electrolyte permeated into the voids of the polyolefin films during the cell fabrication. The symmetric configuration was encapsulated in a 2032 type coin cell. For Li transference number determination by electrochemical polarization, a similar procedure was followed, with 2 sheets of Celgard rather than 4. For the battery tests, [Li metal anode | electrolyte | $LiCoO_2$ cathode] coin cells were constructed, and galvanostatic charge-discharge measurements were carried out. The cathode was composed of $LiCoO_2$ (80 wt.%, AGC Seimi Chemical) as a cathode-active material, acetylene black (10 wt.%, Denki Kagaku Kogyo) as an electrically conductive additive, and poly(vinylidene fluoride) (10 wt.%, Kureha Chemical) as a binder polymer. These materials were mixed together and thoroughly agitated in *N*-methylpyrrolidone with a homogenizer. The obtained slurry was applied with an automatic applicator onto an Al foil, and the resulting cathode sheet was dried at 80 °C for 12h. Then, the cathode sheet was then cut into a disk (16 mm diameter) and compressed at 50 MPa followed by drying in a vacuum at 120 °C for 12 h. The thickness of the composite cathode layer on Al foil was 20 μm, and the loading of $LiCoO_2$ was approximately 4 mg cm^{-2}. The cathode sheet, 2 sheets of Celgard 3501, Li salt-SL electrolyte, and a Li metal anode were encapsulated into a 2032-type coin cell in the glove box. Galvanostatic charge–discharge tests were carried out using an automatic charge/discharge instrument (HJ1001SD8, Hokuto Denko) in the voltage range of 3.0−4.2 V at 30 °C.

ASSOCIATED CONTENT

Supporting Information.

This material is available free of charge via the Internet at http://pubs.acs.org.

Tables S1−S15, Figure S1–S23, and MD simulation details (PDF)

Crystallographic information for $LiBF_4$:SL (1:1)

Crystallographic information for Li[FSA]:SL (1:1)

Crystallographic information for $LiClO_4$:SL (1:2)

Full list of authors for references 22, 23 and 34

AUTHOR INFORMATION

Corresponding Author

*Telephone/Fax: +81-45-339-3955. E-mail: mwatanab@ynu.ac.jp

Notes

The authors declare no conflict of interest.

ACKNOWLEDGEMENTS

Mr. Kenta Watanabe for his kind help in measuring PFG-NMR. This study was supported in part by the JSPS KAKENHI (Grant Nos. 16H06368 and 18H03926) from the Japan Society for the Promotion of Science (JSPS) and the Advanced Low Carbon Technology Research and Development Program (ALCA) of the Japan Science and Technology Agency (JST).

References

1. Bockris, J. O. M.; Reddy, A. K. N., *Modern Electrochemistry: Volume 1*. 2nd ed.; Kluwer Academic/Plenum Publishers: New York, 1998.

2. Izutsu, K., *Electrochemistry in Nonaqueous Solutions*. 2nd ed.; Wiley-VCH Verlag GmbH & Co. KGaA: Weinheim, 2009.

3. Robinson, R. A.; Stokes, R. H., *Electrolyte solutions*. Butterworth & Co. Ltd.: Washington, DC, 1959.

4. Xu, K., Nonaqueous Liquid Electrolytes for Lithium-Based Rechargeable Batteries. *Chem. Rev.* **2004,** *104*, 4303–4418.

5. Xu, K., Electrolytes and Interphases in Li-Ion Batteries and Beyond. *Chem. Rev.* **2014,** *114*, 11503-11618.

6. Suo, L.; Hu, Y. S.; Li, H.; Armand, M.; Chen, L., A New Class of Solvent-in-Salt Electrolyte for High-Energy Rechargeable Metallic Lithium Batteries. *Nat. Commun.* **2013,** *4*, 1481.

7. Yamada, Y.; Furukawa, K.; Sodeyama, K.; Kikuchi, K.; Yaegashi, M.; Tateyama, Y.; Yamada, A., Unusual Stability of Acetonitrile-Based Superconcentrated Electrolytes for Fast-Charging Lithium-Ion Batteries. *J. Am. Chem. Soc.* **2014,** *136*, 5039–5046.

8. Yamada, Y.; Usui, K.; Chiang, C. H.; Kikuchi, K.; Furukawa, K.; Yamada, A., General Observation of Lithium Intercalation into Graphite in Ethylene-Carbonate-Free Superconcentrated Electrolytes. *ACS Appl. Mater. Interfaces* **2014,** *6*, 10892–10899.

9. Qian, J.; Henderson, W. A.; Xu, W.; Bhattacharya, P.; Engelhard, M.; Borodin, O.; Zhang, J. G., High Rate and Stable Cycling of Lithium Metal Anode. *Nat. Commun.* **2015,** *6*, 6362.

10. Yamada, Y.; Yamada, A., Superconcentrated Electrolytes to Create New Interfacial Chemistry in Non-Aqueous and Aqueous Rechargeable Batteries. *Chem. Lett.* **2017,** *46*, 1056–1064.

11. Watanabe, M.; Dokko, K.; Ueno, K.; Thomas, M. L., From Ionic Liquids to Solvate Ionic Liquids: Challenges and Opportunities for Next Generation Battery Electrolytes. *Bull. Chem. Soc. Jpn.*, in press, DOI: 10.1246/bcsj.20180216.

12. Yoshida, K.; Nakamura, M.; Kazue, Y.; Tachikawa, N.; Tsuzuki, S.; Seki, S.; Dokko, K.; Watanabe, M., Oxidative-Stability Enhancement and Charge Transport Mechanism in Glyme-Lithium Salt Equimolar Complexes. *J. Am. Chem. Soc.* **2011,** *133*, 13121–13129.

13. Yamada, Y.; Yamada, A., Review—Superconcentrated Electrolytes for Lithium Batteries. *J. Electrochem. Soc.* **2015,** *162*, A2406–A2423.

14. Wang, J.; Yamada, Y.; Sodeyama, K.; Chiang, C. H.; Tateyama, Y.; Yamada, A., Superconcentrated Electrolytes for a High-Voltage Lithium-Ion Battery. *Nat. Commun.* **2016,** *7*, 12032.

15. Xu, K.; Angell, C. A., High Anodic Stability of a New Electrolyte Solvent: Unsymmetric Noncyclic Aliphatic Sulfone. *J. Electrochem. Soc.* **1998,** *145*, L70–L72.

16. Xu, K.; Angell, C. A., Sulfone-Based Electrolytes for Lithium-Ion Batteries. *J. Electrochem. Soc.* **2002,** *149*, A920–A926.

17. Sun, X.-G.; Angell, C. A., New Sulfone Electrolytes for Rechargeable Lithium Batteries. *Electrochem. Commun.* **2005,** *7*, 261–266.

18. Abouimrane, A.; Belharouak, I.; Amine, K., Sulfone-Based Electrolytes for High-Voltage Li-Ion Batteries. *Electrochem. Commun.* **2009,** *11*, 1073–1076.

19. Sun, X.; Angell, C. A., Doped Sulfone Electrolytes for High Voltage Li-Ion Cell Applications. *Electrochem. Commun.* **2009,** *11*, 1418–1421.

20. Lee, S.-Y.; Ueno, K.; Angell, C. A., Lithium Salt Solutions in Mixed Sulfone and Sulfone-Carbonate Solvents: A Walden Plot Analysis of the Maximally Conductive Compositions. *J. Phys. Chem. C* **2012,** *116*, 23915–23920.

21. Xue, L.; Ueno, K.; Lee, S.-Y.; Angell, C. A., Enhanced Performance of Sulfone-Based Electrolytes at Lithium Ion Battery Electrodes, including the $LiNi_{0.5}Mn_{1.5}O_4$ High Voltage Cathode. *J. Power Sources* **2014,** *262*, 123–128.

22. Alvarado, J.; Schroeder, M. A.; Zhang, M.; Borodin, O.; Gobrogge, E.; Olguin, M.; Ding, M. S.; Gobet, M.; Greenbaum, S.; Meng, Y. S.; et al., A Carbonate-Free, Sulfone-Based Electrolyte for High-Voltage Li-Ion Batteries. *Mater. Today* **2018,** *21*, 341–353.

23. Ren, X.; Chen, S.; Lee, H.; Mei, D.; Engelhard, M. H.; Burton, S. D.; Zhao, W.; Zheng, J.; Li, Q.; Ding, M. S.; et al., Localized High-Concentration Sulfone Electrolytes for High-Efficiency Lithium-Metal Batteries. *Chem* **2018,** *4*, 1877–1892.

24. Hayamizu, K.; Aihara, Y.; Arai, S.; Martinez, C. G., Pulse-Gradient Spin-Echo ^1H, ^7Li, and ^{19}F NMR Diffusion and Ionic Conductivity Measurements of 14 Organic Electrolytes Containing $LiN(SO_2CF_3)_2$. *J. Phys. Chem. B* **1999,** *103*, 519-524.

25. Hayamizu, K.; Akiba, E.; Bando, T.; Aihara, Y., ^1H, ^7Li, and ^{19}F nuclear magnetic resonance and ionic conductivity studies for liquid electrolytes composed of glymes and polyetheneglycol dimethyl ethers of $CH_3O(CH_2CH_2O)_nCH_3$ (n=3–50) doped with $LiN(SO_2CF_3)_2$. *J. Chem. Phys.* **2002,** *117*, 5929-5939.

26. Zhang, C.; Ueno, K.; Yamazaki, A.; Yoshida, K.; Moon, H.; Mandai, T.; Umebayashi, Y.; Dokko, K.; Watanabe, M., Chelate Effects in Glyme/Lithium Bis(trifluoromethanesulfonyl)amide Solvate Ionic Liquids. I. Stability of Solvate Cations and Correlation with Electrolyte Properties. *J. Phys. Chem. B* **2014,** *118*, 5144–5153.

27. Kameda, Y.; Umebayashi, Y.; Takeuchi, M.; Wahab, M. A.; Fukuda, S.; Ishiguro, S.; Sasaki, M.; Amo, Y.; Usuki, T., Solvation Structure of Li^+ in Concentrated $LiPF_6$-Propylene Carbonate Solutions. *J. Phys. Chem. B* **2007,** *111*, 6104–6109.

28. Roobottom, H. K.; Jenkins, H. D. B.; Passmore, J.; Glasser, L., Thermochemical Radii of Complex Ions. *J. Chem. Educ.* **1999,** *76*, 1570–1573.

29. Ue, M.; Murakami, A.; Nakamura, S., A Convenient Method to Estimate Ion Size for Electrolyte Materials Design. *J. Electrochem. Soc.* **2002,** *149*, A1385–A1388.

30. Katon, J. E.; Feairheller, W. R., The Vibrational Spectra and Molecular Configuration of Sulfolane. *Spectrochim. Acta* **1965,** *21*, 199–201.

31. Seo, D. M.; Boyle, P. D.; Allen, J. L.; Han, S.-D.; Jónsson, E.; Johansson, P.; Henderson, W. A., Solvate Structures and Computational/Spectroscopic Characterization of $LiBF_4$ Electrolytes. *J. Phys. Chem. C* **2014,** *118*, 18377–18386.

32. Chabanel, M.; Legoff, D.; Touaj, K., Aggregation of Perchlorates in Aprotic Donor Solvents. Part 1.—Lithium and Sodium Perchlorates. *J. Chem. Soc., Faraday Trans.* **1996,** *92*, 4199–4205.

33. Bruce, P. G., Ed. *Solid State Electrochemistry*. Cambridge University Press: 1997.

34. Zhang, Z.; Shao, Y.; Lotsch, B.; Hu, Y.-S.; Li, H.; Janek, J.; Nazar, L. F.; Nan, C.-W.; Maier, J.; Armand, M.; et al., New Horizons for Inorganic Solid State Ion Conductors. *Energy Environ. Sci.* **2018,** *11*, 1945-1976.

35. Forsyth, M.; Sun, J.; Macfarlane, D. R.; Hill, A. J., Compositional Dependence of Free Volume in PAN/$LiCF_3SO_3$ Polymer-in-Salt Electrolytes and the Effect on Ionic Conductivity. *J. Polym. Sci., Part B: Polym. Phys.* **2000,** *38*, 341–350.

36. Florjańczyk, Z.; Zygadło-Monikowska, E.; Wieczorek, W.; Ryszawy, A.; Tomaszewska, A.; Fredman, K.; Golodnitsky, D.; Peled, E.; Scrosati, B., Polymer-in-Salt Electrolytes Based on Acrylonitrile/Butyl Acrylate Copolymers and Lithium Salts. *J. Phys. Chem. B* **2004,** *108*, 14907–14914.

37. Brinkkotter, M.; Giffin, G. A.; Moretti, A.; Jeong, S.; Passerini, S.; Schonhoff, M., Relevance of Ion Clusters for Li Transport at Elevated Salt Concentrations in [Pyr_{12O1}][FTFSI] Ionic Liquid-Based Electrolytes. *Chem. Commun.* **2018,** *54*, 4278–4281.

38. Callsen, M.; Sodeyama, K.; Futera, Z.; Tateyama, Y.; Hamada, I., The Solvation Structure of Lithium Ions in an Ether Based Electrolyte Solution from First-Principles Molecular Dynamics. *J. Phys. Chem. B* **2017,** *121*, 180–188.

39. Forsyth, M.; Yoon, H.; Chen, F.; Zhu, H.; MacFarlane, D. R.; Armand, M.; Howlett, P. C., Novel Na^+ Ion Diffusion Mechanism in Mixed Organic–Inorganic Ionic Liquid Electrolyte Leading to High Na^+ Transference Number and Stable, High Rate Electrochemical Cycling of Sodium Cells. *J. Phys. Chem. C* **2016,** *120*, 4276–4286.

40. Seo, D. M.; Borodin, O.; Balogh, D.; O'Connell, M.; Ly, Q.; Han, S.-D.; Passerini, S.; Henderson, W. A., Electrolyte Solvation and Ionic Association III. Acetonitrile-Lithium Salt Mixtures–Transport Properties. *J. Electrochem. Soc.* **2013,** *160*, A1061–A1070.

41. Yim, C.-H.; Tam, J.; Soboleski, H.; Abu-Lebdeh, Y., On the Correlation between Free Volume, Phase Diagram and Ionic Conductivity of Aqueous and Non-Aqueous Lithium Battery Electrolyte Solutions over a Wide Concentration Range. *J. Electrochem. Soc.* **2017,** *164*, A1002–A1011.

42. Newman, J.; Thomas-Alyea, K. E., *Electrochemical Systems*. 3rd ed.; John Wiley & Sons: 2004.

43. Diederichsen, K. M.; McShane, E. J.; McCloskey, B. D., Promising Routes to a High Li^+ Transference Number Electrolyte for Lithium Ion Batteries. *ACS Energy Lett.* **2017,** *2*, 2563–2575.

44. Tokuda, H.; Hayamizu, K.; Ishii, K.; Abu Bin Hasan Susan, M.; Watanabe, M., Physicochemical Properties and Structures of Room Temperature Ionic Liquids. 1. Variation of Anionic Species. *J. Phys. Chem. B* **2004,** *108*, 16593–16600.

45. Stejskal, E. O.; Tanner, J. E., Spin Diffusion Measurements: Spin Echoes in the Presence of a Time-Dependent Field Gradient. *J. Chem. Phys.* **1965,** *42*, 288–292.

46. Sheldrick, G. M., SHELXT - Integrated Space-Group and Crystal-Structure Determination. *Acta Crystallogr. Sect. A: Found. Crystallogr.* **2015,** *71*, 3–8.

47. Sheldrick, G. M., Crystal Structure Refinement with SHELXL. *Acta Crystallogr. Sect. C: Cryst. Struct. Commun.* **2015,** *71*, 3–8.

TOC Graphic

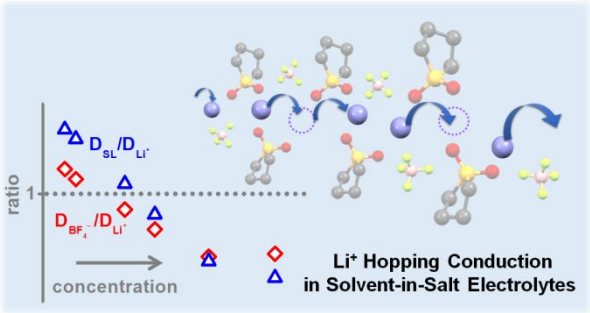
ratio
1
D_{SL}/D_{Li^+}
$D_{BF_4^-}/D_{Li^+}$
concentration
Li^+ Hopping Conduction
in Solvent-in-Salt Electrolytes